Non-uniform seasonal warming regulates vegetation greening and atmospheric CO_2 amplification over northern lands

Non-uniform seasonal warming regulates vegetation greening and atmospheric CO_2 amplification over northern lands

Zhao Li[1,2], Jianyang Xia[1,2,*], Anders Ahlström[3,4], Annette Rinke[5,6], Charles Koven[7], Daniel J. Hayes[8], Duoying Ji[5], Geli Zhang[9], Gerhard Krinner[10,11], Guangsheng Chen[8], Wanying Cheng[1,2], Jinwei Dong[9,12,13], Junyi Liang[9,14], John C. Moore[5], Lifen Jiang[15], Liming Yan[1,2], Philippe Ciais[16], Shushi Peng[10,11,16,17], Ying-Ping Wang[18], Xiangming Xiao[12,19], Zheng Shi[9], A. David McGuire[20], Yiqi Luo[15]

[1]Tiantong National Station of Forest Ecosystem and Research Center for Global Change and Ecological Forecasting, School of Ecological and Environmental Sciences, East China Normal University, Shanghai 200241, China; [2]Institute of Eco-Chongming (IEC), 3663 N. Zhongshan Rd., Shanghai 200062, China; [3]Department of Physical Geography and Ecosystem Science, Lund University, 223 62 Lund, Sweden; [4]Department of Earth System Science, School of Earth, Energy and Environmental Sciences, Stanford University, 473 Via Ortega, Stanford, CA, 94305, USA; [5]College of Global Change and Earth System Science, Beijing Normal University, Beijing, China; [6]Alfred Wegener Institute Helmholtz Centre for Polar and Marine Research, Potsdam, Germany; [7]Lawrence Berkeley National Laboratory, Berkeley, CA, USA; [8]School of Forest Resources, University of Maine, Orono, ME 04469, USA; [9]Department of Microbiology and Plant Biology, University of Oklahoma, OK, 73019, USA; [10]CNRS, Laboratoire de Glaciologie et Géophysique de l'Environnement (LGGE), 38041 Grenoble, France; [11]Université Grenoble Alpes, LGGE, 38041 Grenoble, France; [12]Department of Microbiology and Plant Biology, Center for Spatial Analysis, University of Oklahoma, OK 73019, USA; [13]Institute of Geographic Science and Natural Resources Research, Chinese Academy of Sciences, Beijing, China; [14]Environmental Sciences Division & Climate Change Science Institute, Oak Ridge National Laboratory, Oak Ridge, TN 37830, USA; [15]Department of Biological Sciences, Northern Arizona University, Flagstaff, Arizona; [16]Laboratoire des Sciences du Climat et de l'Environnement, CEA-CNRS-UVSQ, UMR8212, 91191 Gif-sur-Yvette, France; [17]College of Urban and Environmental Sciences Peking University , Beijing, China; [18]CSIRO Oceans and Atmosphere, PMB 1, Aspendale, Victoria 3195, Australia; [19]School of Life Sciences, Fudan University, Shanghai, 200433, China; [20] Institute of Arctic Biology, University of Alaska Fairbanks, Fairbanks, AK, USA

[*]Corresponding author: Jianyang Xia (jyxia@des.ecnu.edu.cn)

Revised Manuscript for *Environmental Research Letters*

Key Points:

- The increasing trend of the atmospheric CO_2 amplitude slowed down during mid-1990s to mid-2000s.
- The asymmetric response of vegetation growth to spring and autumn warming is an important driver for the change in seasonality of atmospheric CO_2.
- A better representation of the autumn phenology would improve the models' performance on the seasonal cycle of atmospheric CO_2.

Abstract

The enhanced vegetation growth by climate warming plays a pivotal role in amplifying the seasonal cycle of atmospheric CO_2 at northern lands (>50ºN) since 1960s. However, the correlation between vegetation growth, temperature and seasonal amplitude of atmospheric CO_2 concentration have become elusive with the slowed increasing trend of vegetation growth and weakened temperature control on CO_2 uptake since late 1990s. Here, based on in-situ atmospheric CO_2 concentration records from the Barrow observatory site, we found a slowdown in the increasing trend of the atmospheric CO_2 amplitude from 1990s to mid-2000s. This phenomenon was associated with the paused decrease in the minimum CO_2 concentration ($[CO_2]_{min}$), which was significantly correlated with the slowdown of vegetation greening and growing-season length extension. We then showed that both the vegetation greenness and growing-season length were positively correlated with spring but not autumn temperature over the northern lands. Furthermore, such asymmetric dependences of vegetation growth upon spring and autumn temperature cannot be captured by the state-of-art terrestrial biosphere models (TBMs). These findings indicate that the responses of vegetation growth to spring and autumn warming are asymmetric, and highlight the need of improving autumn phenology in the models for predicting seasonal cycle of atmospheric CO_2 concentration.

1 Introduction

Temporal dynamics of atmospheric CO_2 concentration, climate and terrestrial carbon (C) cycle are strongly linked in the present (Schneising *et al* 2014) and past (Montañez *et al* 2016) Earth systems. For example, the recent inter-annual variability of atmospheric CO_2 growth rate is largely caused by fluctuations in terrestrial CO_2 uptake (Myneni *et al* 1997, Keenan *et al* 2016), which is mainly driven by variations in climate (Poulter *et al* 2014, Ahlström *et al* 2015, Jung *et al* 2017). On the decadal scale, an increasing amplitude of the atmospheric CO_2 seasonal cycle at northern high latitudes has been observed since 1960s (Bacastow *et al* 1985, Kelling *et al* 1996, Randerson *et al* 1997, Graven *et al* 2013), e.g., about 0.53% yr^{-1} at the Point Barrow (BRW) during 1971-2011 (Forkel *et al* 2016). Although the major contributors to such trend of seasonal atmospheric CO_2 amplitude are still in debate (Gray *et al* 2014, Zeng *et al* 2014, Ito *et al* 2016, Wenzel *et al* 2016, Piao *et al* 2017a), the associated increases in mean annual temperature (MAT) and vegetation growth has been recognized as one important driver (Forkel *et al* 2016, Piao *et al* 2017a, Gonsamo *et al* 2017, Yuan *et al* 2018). Recently, non-uniform warming trends among seasons have been detected over the northern lands (Xu *et al* 2013, Xia et al 2014). Given that climate warming in different seasons would influence vegetation growth differently (Xu *et al* 2013, Xia *et al* 2014, Cai *et al* 2016), the role of seasonal non-uniform warming in affecting the vegetation growth as well as the recent changes of the atmospheric CO_2 amplitude remains unclear.

Some recent evidence has implied weakening correlations of MAT with vegetation growth and atmospheric CO_2 concentration in the past three decades. First, the MAT across the northern high latitudes has kept rising whereas vegetation greenness has begun to decline since late 1990s (Bhatt *et al* 2013, Jeong *et al* 2013). Second, the advanced spring phenology in response to climate warming has been reported to diminish at northern high latitudes over the last two decades (Fu *et al* 2015, Wang *et al* 2015). Third, a weakening inter-annual correlation of temperature with vegetation greenness (Piao *et al* 2014) or spring ecosystem CO_2 uptake (Piao *et al* 2017b) has been detected at northern latitudes during recent years. In northern temperate ecosystems, a negative correlation between the atmospheric CO_2 amplitude and

temperature anomalies during 2000s has been found through the analysis of space-borne atmospheric CO_2 measurements (Schneising *et al* 2014). Thus, it is important to examine how the temperature changes in different seasons have contributed to such weakening correlations of MAT with vegetation growth and seasonal CO_2 amplitude in recent years.

In this study, we investigated the relationships between changes in the seasonal CO_2 amplitude, vegetation greenness and seasonal air temperature in northern lands (>50ºN) during the last three decades. The analyses were based on long-term monitoring records of atmospheric CO_2, global gridded climate datasets, and satellite-derived Normalized Difference Vegetation Index (NDVI). We also examined the relationships between temperature and gross primary productivity (GPP) in five terrestrial biosphere models (TBMs), which have been commonly incorporated into Earth system models for future projections of climate and atmospheric changes.

2 Data and Methods

2.1 Atmospheric CO_2 measurements

There are 19 CO_2 measurement sites in the NOAA's Global Greenhouse Gas Reference Network (https://www.esrl.noaa.gov/gmd/ccgg/ggrn.php) and 3 sites in Scripps CO_2 program (http://scrippsco2.ucsd.edu/data/atmospheric_co2/sampling_stations) located at lands over 50º N. Among these sites, only the Barrow observatory (BRW) site recorded the atmospheric CO_2 concentration (i.e., [CO_2]) continuously during 1982-2010. Thus, in this study, the in-situ long-term CO_2 measurements from BRW were regarded as the homogeneous CO_2 concentration in northern lands (>50ºN). The seasonal curve of this [CO_2] record was shown in figure S1.

The in-situ [CO_2] observations at the BRW site were collected hourly. The daily and monthly data provided by NOAA were averaged from the hourly observations. This study used the monthly data to derive the CO_2 amplitude. The anomalies of monthly [CO_2] (i.e., monthly [CO_2] - yearly mean [CO_2]) were first calculated and then were used to derive the maximum (i.e., $[CO_2]_{max}$) and minimum (i.e., $[CO_2]_{min}$) monthly [CO_2] in each year. The difference between $[CO_2]_{max}$ and $[CO_2]_{min}$ was defined as the CO_2 amplitude ($[CO_2]_{amplitude}$).

To avoid the biases of various processing algorithms, we collected the estimates of $[CO_2]_{amplitude}$ from Forkel *et al* (2016) and the GLOBALVIEW products (figure S2). In Forkel *et al*. (2016), the time series of daily $[CO_2]$ records were first fitted with polynomial and harmonics functions and then de-trended with the Fast Fourier Transformation (FFT) method (Thoning *et al* 1989, Thoning *et al* 2015). In each calendar year, the $[CO_2]_{amplitude}$ was calculated as the peak-to-trough difference of the de-trended seasonal cycle. The data in the GLOBALVIEW-CO_2 product has already been smoothed, interpolated and extrapolated (Masane KA & Tans PP 1995). GLOBALVIEW-CO_2 provides observations at 7-day intervals. We obtained its $[CO_2]_{amplitude}$ as the difference between the maximum and minimum weekly CO_2 data in each calendar year. According to the Theil-Sen analysis, the long-term trends of $[CO_2]_{amplitude}$ were consistent among these processing methods (figure S2).

2.2 Temperature analysis

The temperature trends were analyzed based on the latest version of the CRU temperature data (CRU TS4.0). It is gridded with a spatial resolution of 0.5°×0.5° at a monthly time step. This product is gridded using the Angular-distance weighting (ADW) interpolation (Harris & Jones 2017) based on the observations collected from 2600 stations worldwide (Harris *et al* 2014). The CRU climate products have been widely used for phenology analysis and for driving different types of ecosystem models (Koven *et al* 2011, Fu *et al* 2014, Xia *et al* 2017). In this study, seasonal temperature was averaged from monthly temperature following the definition of four seasons: Spring, March–May; Summer, June–August; Autumn, September–November; Winter, December–February. Besides, MAT of a given year was defined as the average of the monthly temperature from January to December. The Theil-Sen estimator and Mann-Kendall trend test were applied in detecting the temporal trends of the seasonal temperature (see more details at the Section 2.6).

2.3 Satellite derived NDVI

The normalized difference vegetation index (NDVI) is widely used as an indicator for vegetation productivity (Myneni *et al* 1997, Zhou *et al* 2001). It is calculated as the normalized ratio between near infrared and red reflectance bands (Tucker *et al* 1979, Tucker *et al* 2005).

The NDVI used in this study is from the Advanced Very High Resolution Radiometer (AVHRR) sensors, which has the longest record of continuous satellite data since 1981. Here, we used the newest version of GIMMS NDVI dataset (NDVI3g) (Tucker *et al* 2005, Pinzon *et al* 2014). It is a global product at spatial resolution of ~ 8 ×8 km and temporal resolution of 15 days. The NDVI3g has been widely used for analyzing vegetation changes in recent years (Tucker *et al* 2005, Peng *et al* 2013, Wang *et al* 2014). The maximum value composites (MVC) method (Holben 1986) was applied to merge segmented data strips to half-monthly values. To lessen the impacts of sparse soils and snows on vegetation, following zhang *et al.* (2013), the areas with multiyear average NDVI less than 0.1 in the northern lands (>50°N) were removed from the analysis. Moreover, only the half-monthly NDVI from January to September were used to derive the phenology indices (i.e., start and end of growing season length, see section 2.4).

The sum of monthly NDVI from January to December in a certain year was regard as the yearly NDVI. Note that the illegitimate signals of the half-monthly NDVI data (i.e., NDVI <0.1) were filtered. Regional NDVI used in the trend analysis were averaged from the grids of the northern lands (>50°N). Before calculating the sensitivity of NDVI to MAT and the partial correlation between NDVI and seasonal temperature (see section 2.6), yearly NDVI data were resampled to raster of 0.5°×0.5°, to couple with the CRU temperature data.

2.4 Method of determining growing season length

Growing season length (GSL) was calculated as the difference between the start (SOS) and end (EOS) of growing season. The SOS and EOS were retrieved from the seasonal NDVI curve in each year based on the NDVI green-up thresholds, which were determined from the rate of seasonal changes in the multiyear mean NDVI (Piao *et al* 2006, 2011; Zhang *et al* 2013). More specifically, there were six steps in the determination of GSL. First, we calculated the seasonal curve of multiyear mean NDVI from 1982 to 2010 for each land grid cell and obtained the changing rate of NDVI ($NDVI_{ratio}$) as:

$$NDVI_{ratio}(t) = [NDVI(t+1) - NDVI(t)]/[NDVI(t)]$$

where t is time throughout the year with an interval of 15 days. Then, after removing evident noise in the multiyear mean time-series curve of NDVI for each land grid cell, we performed a

least-square regression analysis on the curves from January to September and from July to December for determining the NDVI thresholds of SOS and EOS, respectively, with an inverted parabola equation:

$$NDVI = a + a_1x + a_2x^2 + \cdots + a_nx^n$$

where x is the Julian days and n is 6. The corresponding NDVI(t) with the maximum or minimum $NDVI_{ratio}$ was used as the NDVI threshold for determining SOS or EOS, respectively. Next, we performed a least-square regression analysis on the NDVI time-series curve in each year for each pixel after removing noise in the two different periods. After that, the SOS and EOS were identified from the fitted NDVI seasonal curves and their NDVI thresholds, by selecting the day when the fitted NDVI curve first reached the NDVI threshold. Finally, the GSL in each year for each land cell was calculated from the difference between EOS and SOS. The method in this study had been validated by ground-based phenological data in Tibetan Plateau (Zhang *et al* 2013) and has been widely used for detecting phenological changes in various regions (Piao *et al* 2006, Piao *et al* 2011, Zhang *et al* 2013).

2. 5 Simulated GPP by terrestrial biosphere models.

Outputs of annual GPP from five terrestrial biosphere models (TBMs) which provided all the land cells above the 50°N in the model integration group of the Permafrost Carbon Network (http://www.permafrostcarbon.org/) were analyzed in this study. The five TBMs are UVic (Peter 2001, Matthews et al. 2004), CoLM (Dai *et al* 2003, Ji *et al* 2014), CLM4.5 (Keith W. Oleson *et al* 2003), TEM604 (Hayes *et al* 2011) and ORCHIDEE (Krinner *et al* 2005). Details about these TBMs were listed in table S1. The simulation protocol and model's driving data have been described in previous studies (Rawlins *et al* 2015, McGuire *et al* 2016, Peng *et al* 2016). A flux-tower-based GPP database was also used in this study. It was up-scaled from FLUXNET observations (44 sites locating in the lands northern 50°N) of carbon dioxide, energy and water fluxes with the machine learning technique of model tree ensembles (MTE, Jung *et al* 2011). The MTE GPP is a global gridded product with a resolution of 0.5° × 0.5°. This product has been widely used as benchmarks to evaluate model performance in recent years (Anav *et al* 2013, Tjiputra *et al* 2013, Peng *et al* 2015, Xia *et al* 2017).

2.6 Statistical analyses.

We estimated the linear trends of the CO_2 indices (i.e., $[CO_2]_{amplitude}$, $[CO_2]_{max}$ and $[CO_2]_{min}$), vegetation and temperature using a non-parametric Theil-Sen estimator over each time period. The significance of the trend was computed by the Mann-Kendall trend test. Comparing with the ordinary least squares estimation, the Theil-Sen estimator and Mann-Kendall trend test is less sensitive to outliers (Fernandes & Leblanc 2005, Wang *et al* 2018). The temporal anomalies were used for the linear-trend analyses. This analysis can provide both trend and its level of significance (i.e., the *P* value that quantifies the probability of whether the trend is statistically significant from zero) for each period.

The moving-window method was used to detect whether the increasing trends of CO_2 indices are persistent. Comparing with the piecewise linear fitting method, it less depends on the results of single linear segment and the interval-length (Schleip *et al* 2008). This method has been used in detecting the changes of growing-season length and its response to climate change on various time scales (Rutishauser *et al* 2007, Schleip *et al* 2008, Jeong *et al* 2011, Fu *et al* 2015). Because the results based the moving-window analysis may be affected by the window-length (Fu *et al* 2015), we repeated the moving-window analyses with 10-year, 15-year and 20-year lengths.

The temporal trends of MAT (Δ_{MAT}), the sensitivity of NDVI to temperature (γ_{NDVI}), and the sensitivity of CO_2 amplitude to temperature ($\gamma_{[CO_2]_{amplitude}}$) in the periods of 1982-2010 and 1993-2007 were calculated in each grid cell. The γ_{NDVI} and $\gamma_{[CO_2]_{amplitude}}$ were derived from the slope of linear regressions, representing the changes of NDVI and $[CO_2]_{amplitude}$ with per degree change of MAT. One-way ANOVA was used to estimate their differences between 1982-2010 and 1993-2007. All the analyses were applied in ***R*** (http://www.r-project.org/).

Partial correlation analyses were applied to exclude the impacts of the co-varying factors. For example, in calculating the impact of spring temperature on SOS, spring precipitation, spring solar radiation and last-year's autumn temperature were set as the controlling variables. Autumn precipitation, autumn solar radiation and spring temperature were set as the controlling

variables to quantify the impact of autumn temperature on EOS. Similar method was used to detect the impact of spring and autumn temperature on annual NDVI and modeled GPP by replacing the seasonal precipitation and solar radiation with annual values. All the data were aggregated to the $0.5^{o} \times 0.5^{o}$ resolution. The precipitation data were derived from the CRU TS4.0 data set (Harris *et al* 2014) and the radiation data was from the Terrestrial Hydrology Research Group at Princeton University (Sheffield *et al* 2006).

3 Results and Discussion

3.1 The temporal changes of atmospheric CO_2 seasonal cycle and vegetation greenness

We first examined the trends of the measured annual CO_2 amplitude ($[CO_2]_{amplitude}$) at Point Barrow, Alaska (BRW, 71°N). The non-parametric Theil-Sen estimator showed that the increasing trends of the $[CO_2]_{amplitude}$ at the BRW (0.075 ppm yr^{-1}, P <0.05; figure 1(a)) were associated with the decreasing $[CO_2]_{min}$ (-0.058 ppm yr^{-1}, P <0.05) rather than the enhancing $[CO_2]_{max}$ (0.016 ppm yr^{-1}, P =0.17) from 1982 to 2010. The 10-year moving windows show that the increasing rates of the CO_2 amplitude was slower around 2000 (figure 1(a) and table S2). To avoid the biases from different time-intervals for trend estimation, we also detected the trends with 15-year (figure S3) and 20-year (figure S4) moving windows. The results also showed that the trends of $[CO_2]_{amplitude}$ from mid-1990 to mid-2000 (e.g., 0.03 ppm yr^{-1}, P =0.55, 1993-2007) (figure S4(a) and table S4) were significantly slower than those during other periods. A recent study which integrated the CO_2 records from multiple sites also has showed a stalled trend in the seasonality of atmospheric CO_2 during the same period (Yuan *et al* 2018).

A slowdown of vegetation greening since mid-1990s was also observed by our analysis on the dynamics of NDVI (figure 1(b) and figure S5(d)). This finding is consistent with the results from recent analyses on vegetation dynamics over the pan-Arctic tundra (Bhatt *et al* 2013, Jeong *et al* 2013). Both the MTE GPP (figure S5(e)) and the ground-based measurements of growing-season net ecosystem CO_2 exchange (figure S5(f)) showed similar trends since 1990s. These lines of evidences together suggest that the increasing trend of the growing-season CO_2 uptake has weakened from 1990s to mid-2000s in northern ecosystems.

Meanwhile, a weak but significant linear relationship between average NDVI over the northern lands (>50ºN) and $[CO_2]_{min}$ at the BRW site was observed during 1982-2010 (r = -0.47, P <0.05; figure 1(b)). The synchronous changes of $[CO_2]_{amplitude}$ with $[CO_2]_{min}$ (figure S5(a), (b) and (c)) and NDVI (figure 1) imply that the long-term positive trend of $[CO_2]_{amplitude}$ is, at least in part, driven by photosynthetic CO_2 uptake or vegetation growth (Forkel *et al* 2016, Wenzel *et al* 2016).

3.2 The asymmetric responses of vegetation growth to spring and autumn warming

An increasing body of research has shown a non-linear response or reduced sensitivity of vegetation growth to rising MAT over high latitudes in recent years (Bhatt *et al* 2013, Jeong *et al* 2013, Piao *et al* 2014). As shown by figure 2, although the MAT increased even faster from mid-1990s to mid-2000s (e.g., 1993-2007) than the whole period of 1982-2010, the sensitivities of $[CO_2]_{amplitude}$ and NDVI to MAT were lower during that period than 1982-2010. Given the fact that temperature in different seasons has non-uniform impacts on vegetation growth (Xia *et al* 2014), we further analyzed the changes of seasonal temperatures based on the CRU temperature datasets (see Methods). As shown by figure 3(b), the fastest warming season was spring during 1985-1999 (+0.12 ºC $year^{-1}$) but then changed to autumn during mid-1990s to mid-2000s (e.g., +0.11 ºC $year^{-1}$ in 1993-2007, table S4). It indicates that a better understanding of the relationship between the seasonal temperature changes and vegetation growth is needed to explain the slowdown of $[CO_2]_{amplitude}$ from 1990s to mid-2000s.

The variation of NVDI during 1982-2010 in northern ecosystems depends substantially on the GSL on both grid and regional scales (figure 1(b) and figure S6). Further partial correlation analysis showed that the SOS (partial r = -0.36) was more dependent on temperature change than the EOS (partial r = 0.018, figure 3(c) and figure S7). During 1982-2010, the SOS was advanced by 2.15 day $ºC^{-1}$ with spring warming, whereas warming in autumn only delayed EOS by 0.80 day $ºC^{-1}$ in northern ecosystems. As a result, the advancing rate of SOS over the moving 15 years has decreased but the extending rate of EOS was not significantly increased during 1982-2010 (figure S8 and table S5). Meanwhile, the increasing rate of NDVI until it stalled in mid-1990s is driven by warming-induced increase in spring and early summer NDVI

along with the advancement of SOS (figure S8), for which spring warming has stalled after mid-1990s. It has contributed to the decline in the rate of $[CO_2]_{amplitude}$ increase since the mid-1990s. These results together suggest that the non-uniform warming between spring and autumn during mid-1990s and mid-2000s (figure 3(b)) could be an important driving factor for the slowdown of expanding GSL, greening vegetation and the decreasing $[CO_2]_{min}$. This can qualitatively explain the pause in the enhancement of $[CO_2]_{amplitude}$ (figure 1(a)).

3.3 The response of vegetation productivity to spring and autumn warming in current terrestrial biosphere models

We examined whether TBMs that have been focusing on simulation of C dynamics in northern latitudes can adequately represent the differential impacts of spring and autumn warming on vegetation productivity. The ensemble output of GPP from five TBMs (CLM4.5, CoLM, ORCHIDEE, TEM6 and UVic; table S1) and a flux-based GPP dataset (MTE) were analyzed (figure 4). The dependence of modeled GPP variations on spring-temperature change (with the inter-model mean partial r as 0.57 under the significant level of P <0.05) is comparable with that of the MTE GPP (partial r = 0.53, P <0.05) as well as that of NDVI (partial r = 0.49, P <0.05; figure 4(b) and figure S9). However, the dependences of GPP variations on autumn-temperature change is more positive in the models (inter-model mean partial r = 0.31, P <0.05) than the MTE GPP (partial r = -0.04, P <0.05) and NDVI (partial r = -0.16, P <0.05; figure 4(b) and figure S10). This mismatch between modeling and data-oriented results indicates that the current TBMs overestimate the positive impact of rising MAT on ecosystem CO_2 uptake in the autumn.

As the land biogeochemical component in most Earth system models is similar to the TBMs in this study, it is still challenging to accurately simulate the seasonal cycle of atmospheric CO_2. The findings of this study suggest that a better representation of the warming impacts on autumn phenology could partially improve the models' performance. However, the autumn phenology is diversely represented in different models. For example, leaf senescence in the ORCHIDEE model is simulated as the timing when monthly temperature falls below a given number, which varies with plant function type (Krinner *et al* 2005). In the TEM, growing

season ended when the soil temperature is lower than the frozen point. However, leaf-senescence events are collectively affected by not only temperature but also day length (Ballantyne *et al* 2017), radiation (Bauerle *et al* 2012) and even spring phenology (Liu *et al* 2016, Keenan & Richardson 2015). In fact, the poor representation of autumn phenology by the models has been raised in some previous studies (Richardson *et al* 2010, 2012; Keenan & Richardson 2015). Thus, combining the different types of phenological data (e.g., Richardson *et al* 2018) with better phenology models could be helpful to improve the simulation of the seasonal cycle of atmospheric CO_2 at high latitudes in Earth system models.

3.4 The role of the non-uniform warming in regulating the seasonal atmospheric CO_2 cycle

This study highlights that the asymmetric responses of vegetation growth to spring and autumn warming is an important driver for the decadal changes in the seasonality of atmospheric CO_2. In spring, solar radiation is not limiting as temperature (Tanja *et al* 2003). Thus, spring warming extends the growing season length by advancing the onset of plant photosynthesis (Piao *et al* 2008), leading to the increasing vegetation productivity and the decreasing $[CO_2]_{min}$ of the atmospheric CO_2 seasonal cycle. In autumn, solar radiation can obstruct the accumulation of abscisic acid (Gepstein & Thimann 1980) and substantially delay the timing of leaf senescence. Photoperiod is a more proximal factor than temperature in controlling senescence (Bauerle *et al* 2012). Thus, autumn warming has a neutral impact on vegetation productivity (figure 3(c)) over the northern lands.

Warming in autumn as well as in spring could potentially enhance the peak of atmospheric CO_2 seasonal cycle by stimulating the respiratory processes of plants and soil microorganisms (Piao *et al* 2008, 2017a). As shown by the FLUXCOM database (Jung *et al* 2017), the increasing trends of total ecosystem respiration during both growing and non-growing seasons were significantly larger in mid-1990s to mid-2000s (e.g., 1993-2007) than 1982-2010 (figure S11). This result is consistent with previous findings that the warming induced increases in respiration could partially cancel out the impact of enhanced photosynthesis on the atmospheric CO_2 seasonality in North Hemisphere (Gonsamo *et al* 2017,

Jeong *et al* 2018). However, further conclusions are limited by quantifying the contributions of increased respiration to the slowdown of CO_2 amplitude since mid-1990s. Future studies could improve on the present analysis through breaking the limitation.

Both spring and autumn are likely to keep warming in future scenarios (IPCC, 2013), and further warming could trigger some limitations on vegetation productivity. For example, early spring warming may slow the fulfillment of chilling requirement for spring leaf phenology and thus delay the SOS (Yu *et al* 2010, Fu *et al* 2015, Vitasse *et al* 2018). The spring warming induced advancement of leaf unfolding date could increase the risk of frost damage to buds (Inouye 2008) and decrease soil water availability for subsequent peak productivity (Buermann *et al* 2013). Autumn warming may cause more cloudy days with less radiation (Vesala *et al* 2010), which may accelerate the ending of growing season (Bauerle *et al* 2012). Meanwhile, warm autumns strengthen the evapotranspiration during the late growing season and intensify the stresses of drought on vegetation growth (Barichivich *et al* 2013).

4 Conclusions

This study detected a slowdown of the increase in atmospheric CO_2 amplitude during mid-1990s to mid-2000s. This phenomenon was correlated with the pause of increasing NDVI and advancing SOS across the lands at northern high latitudes during the same period. The changes of vegetation greenness and growing-season length were temporally correlated with the stalled increase in spring temperature since mid-1990s. Warming in autumn was persistent during this period, suggesting that the non-growing season respiration could be more important in governing the future increase in seasonal CO_2 amplitude (Jeong *et al* 2018). These findings emphasize that the asymmetric responses of vegetation growth to spring and autumn warming is important in influencing the change of atmospheric CO_2 amplitude. This study also indicates that global carbon-cycle models need to better represent the phenological response to temperature change for accurately simulating the seasonal cycle of atmospheric CO_2. Overall, this study confirms that the recent non-uniform climate warming among seasons has played an important role in regulating the temporal trends of vegetation growth and atmospheric CO_2 amplification over the northern lands.

Acknowledgments

This work is financially supported by the National Key R&D Program of China (2017YFA0604600), the National Natural Science Foundation (31430015, 41601099, 41630528), the National 1000 Young Talents Program of China, Terrestrial Ecosystem Sciences grant of the US Department of Energy (DE SC0008270), National Science Foundation (NSF) grants (DEB 0743778, DEB 0840964, EPS 0919466, EF 1137293 and IIA-1301789), NASA grant (NNX11AJ35G), and USDA grant (2012-02355). This study was also developed through the activities of the modeling integration team of the Permafrost Carbon Network (PCN, www.permafrostcarbon.org) funded by the National Science Foundation and the U.S. Geological Survey. We appreciate the comments from Dr. Shilong Piao on the early version, and acknowledge the NOAA's Global Greenhouse Gas Reference Network for collecting the long-term records of atmospheric CO_2 concentration. Any use of trade, firm, or product names is for descriptive purposes only and does not imply endorsement by the U.S. Government.

Author information and contributions

The authors declare no competing financial interests. Correspondence should be addressed to J. Xia (jyxia@des.ecnu.edu.cn). JX designed the study and ZL performed the analyses. AR, CK, DJH, DJ, EB, GK, GC, JCM, PC, SP and ADM provided the modeling results. All authors contributed extensively to the writing and discussions.

References

Anav, A., P. Friedlingstein, M. K. L. Bopp, P. Ciais, P. Cox, C. Jones, M. Jung, R. Myneni, and Z. Zhu 2013 Evaluating the land and ocean components of the global carbon cycle in the CMIP5 Earth System Models. *J. Clim* 26 6801–6843.

Ahlström, A., M. R. Raupach, G. Schurgers, B. Smith, A Arneth, M. Jung, M. Reichstein, J. G. Canadell, P. Friedlingstein, A. K. Jain, E. Kato, B. Poulter, S. Sitch, B. D. Stocker, N. Viovy, Y. P. Wang, A. Wiltshire, S. Zaehle and N. Zeng 2015 The dominant role of semi-arid ecosystems in the trend and variability of the land CO_2 sink. *Science* 348 895-899.

Bacastow R. B, C. D. Keeling and T. P. Whorf. 1985 Seasonal Amplitude Increase in Atmospheric CO_2 Concentration at Mauna Loa, Hawaii, 1959-1982. *J. Geophys Res* 90 10539-10540.

Ballantyne, A., W. Smith, W. Anderegg, P. Kauppi, J. Sarmiento, P. Tans, E. Shevliakova, Y. Pan, B. Poulter, A. Anav, P. Friedlingstein, R. Houghton, and S. Running 2017 Accelerating net terrestrial carbon uptake during the warming hiatus due to reduced respiration. *Nature Clim. Change* 7 148-152.

Barichivich, J., K. R. Briffa, R. B. Myneni, Timothy J. Osborn, Thomas M. Melvin, Philippe Ciais, Shilong Piao and C. Tucker 2013 Large-scale variations in the vegetation growing season and annual cycle of atmospheric CO_2 at high northern latitudes from 1950 to 2011. *Glob. Change Biol* 19 3167-3183.

Bauerle, W. L., R. Oren, D. A. Way, Song S. Qian, P. C. Stoy, Peter E. Thornton, Joseph D. Bowden, F. M. Hoffman and R.F. Reynolds 2012 Photoperiodic regulation of the seasonal pattern of photosynthetic capacity and the implications for carbon cycling. *Proc. Natl Acad. Sci. USA* 109 8612-8617.

Belshe. E. F., E. A. Schuur, and B. M. Bolker 2013 Tundra ecosystems observed to be CO_2 sources due to differential amplification of the carbon cycle. *Ecol Lett* 16 1307-1315.

Bhatt. U. S., D. A. Walker, M. K. Raynolds, P. A. Bieniek, H. E. Epstein, J. C. Comiso, Jorge E. Pinzon, C. J. Tucker and I. V. Polyakov 2013 Recent declines in warming and vegetation greening trends over pan-Arctic tundra. *Remote Sensing* 5 4229-4254.

Buermann, W., P. R. Bikash, M. Jung, D. H. Burn, and M. Reichstein. 2013 Earlier springs decrease peak summer productivity in North American boreal forests. *Environ. Res. Lett* 8 024-027.

Cai, Q., Y. Liu, Y. C. Wang, Y. Ma, H. Liu 2016 Recent warming evidence inferred from a tree-ring-based winter-half year minimum temperature reconstruction in northwestern Yichang, South Central China, and its relation to the large-scale circulation anomalies. *Int J Biometeorol* 12 1885-1896.

Dai, Y., X. Zeng, R. E. Dickinson, I Bonan G, Bosilovich M, Denning A, Dirmeyer P, Houser P, Niu G, Oleson K, Schlosser C, Yang Z 2003 The Common Land Model. *B. Am. Meteorol. Soc* 84 1013-1023.

Fernandes, R and S. G. Leblanc 2005. Parametric (modified least squares) and non-parametric (Theil-Sen) linear regressions for predicting biophysical parameters in the presence of measurement errors. *Remote Sens Environ* 95 303–316.

Forkel M., N. Carvalhais, C. Rödenbeck, R. Keeling, M. Heimann, K. Thonicke, S. Zaehle, M. Reichstein 2016 Enhanced seasonal CO_2 exchange caused by amplified plant productivity in northern ecosystems. *Science* 351 696-699.

Fu, Y. H., S. Piao, M. O. Beeck, N. Cong, H. Zhao, Y. Zhang, A. Menzel and I. A. Janssens 2014 Recent spring phenology shifts in western Central Europe based on multiscale observations. *Global Ecol. Biogeogr* 23 1255–1263.

Fu, Y. H., H. Zhao, S. Piao, M. Peaucelle, S. Peng, G. Zhou, P. Ciais, M. Huang, A. Menzel, J. Peñuelas, Y. Song, Y. Vitasse, Z. Zeng and I. A. Janssens 2015 Declining global warming effects on the phenology of spring leaf unfolding. *Nature* 526 104-107.

Gepstein, S., & Thimann, K. V. 1980 Changes in the abscisic acid content of oat leaves during senescence. *Proc. Natl Acad. Sci. USA* 77 2050-2053.

Gonsamo A, Chen JM, Lombardozzi D 2016 Global vegetation productivity response to climatic oscillations during the satellite era. *Global. Change. Biol* 22 3414–3426.

Gonsamo, A., P. Odorico, J. M. Chen, C.Y. Wu and N. Buchmann 2017 Changes in vegetation phenology are not reflected in atmospheric CO_2 and $^{13}C/^{12}C$ seasonality. *Global. Change. Biol* 23 4029-4044.

Graven, H., R. Keeling, S. Piper, S. C. Piper, P. K. Patra, B. B. Stephens, S. C. Wofsy, L. R. Welp, C. Sweeney, P. P. Tans, J. J. Kelley, B. C. Daube, E. A. Kort, G. W. Santoni and J. D. Bent 2013 Enhanced seasonal exchange of CO_2 by northern ecosystems since 1960. *Science* 341 1085-1089.

Gray, J. M, S. Frolking, E. A. Kort, D. K. Ray, C. J. Kucharik, N. Ramankutty and M. A. Friedl 2014 Direct human influence on atmospheric CO_2 seasonality from increased cropland productivity. *Nature* 515 398–401.

Harris, I., Jones, P.D., Osborn, T.J. and Lister D.H 2014 Updated high-resolution grids of monthly climatic observations – the CRU TS3.10 Dataset. *Int. J. Climatol* 34 623–642.

Harris, I.C.and Jones, P.D 2017 University of East Anglia Climatic Research Unit 2017 CRU TS4.00: Climatic Research Unit (CRU) Time-Series (TS) version 4.00 of high-resolution gridded data of month-by-month variation in climate (Jan. 1901- Dec. 2015). Centre for Environmental Data Analysis, 25 August 2017.

Hayes, D.J., A.D. McGuire, D.W. Kicklighter, K.R. Gurney, T.J. Burnside, and J.M. Melillo 2011 Is the northern high latitude land-based CO_2 sink weakening. *Global Biogeochemical Cycles*, 25 GB3018.

Holben BN 1986 Characteristics of maximum-value composite images from temporal AVHRR data. *Int J Remote Sens* 7 1417–1434.

Inouye, D. W. 2008 Effects of climate change on phenology, frost damage, and floral abundance of montane wildflowers. *Ecology* 8 353-362.

IPCC. Stocker TF, Qin D, Plattner G-K, Tignor M, Allen SK, Boschung J, Nauels A, Xia Y, Bex V, Midgley PM, eds. Climate Change 2013: The Physical Science Basis. Contribution of Working Group I to the Fifth Assessment Report of the Intergovernmental Panel on Climate Change. Cambridge, UK/ New York: Cambridge University Press 2013 1535.

Ito, A., M. Inatomi, D. N. Huntzinger, C. Schwalm, A. M. Michalak, R Cook, A W. King, J.F Mao, Y. X. Wei, W. M. Post, W. Wang, M. A. Arain, S. Huang, D. J. Hayes, D M. Ricciuto, X.Y. Shi, M.Y. Huang, H. Lei, H.Q. Tian, C. Q. Lu, J. Yang, Bo Tao, Atul Jain, B Poulter, S.S.Peng, P. Ciais, J. B. Fisher, N. Parazoo, K. Schaefer, C.H. Peng, N. Zeng and F. Zhao 2016 Decadal trends in the seasonal-cycle amplitude of terrestrial CO_2 exchange resulting from the ensemble of terrestrial biosphere models. *Tellus B* 68 28968.

Jeong, S. J., C. H. Ho, H. J. GIM, and M. E. Brown 2011 Phenology shifts at start vs. end of growing season in temperate vegetation over the Northern Hemisphere for the period 1982–2008. *Global. Change. Biol* 17 2385-2399.

Jeong, S. J., C. H. Ho, B. M. Kim, S. Feng, and D. Medvigy 2013 Non-linear response of vegetation to coherent warming over northern high latitudes. *Remote Sens. Lett.* 4 123-130.

Jeong, S. J., A. A. Bloom, D. Schimel, C. Sweeney, N. C. Parazoo, D. Medvigy, G Schaepman-Strub, C Zheng, C. R. Schwalm, D. N. Huntzinger, A. M. Michalak, C. E. Miller Accelerating rates of Arctic carbon cycling revealed by long-term atmospheric CO_2 measurements. 2018 *Science advances* 4 eaao1167.

Ji, D., L. Wang, J. Feng, Q. Wu, H. Cheng, Q. Zhang, J. Yang, W. Dong, Y. Dai, D. Gong, R.-H. Zhang, X. Wang, J. Liu, J. C. Moore, D. Chen, and M. Zhou 2014 Description and basic evaluation of Beijing Normal University Earth System Model (BNU-ESM) version 1. *Geosci. Model. Dev* 7 2039-2064.

Jung, M., M. Reichstein, H. A. Margolis, A. Cescatti, Andrew D. Richardson, M. Altaf Arain, A. Arneth, C. Bernhofer, D. Bonal, J. Chen, D. Gianelle, N, Gobron, G. Kiely, W. Kutsch, G. Lasslop, B. E. Law, A. Lindroth, L. Merbold, L. Montagnani, E. J. Moors, D. Papale, M. Sottocornola, F. Vaccari and C. Williams 2011 Global patterns of land-atmosphere fluxes of carbon dioxide, latent heat, and sensible heat derived from eddy covariance, satellite, and meteorological observations. *J. Geophys. Res. Biogeosci* 116 G001566.

Jung, M M. Reichstein, C. R. Schwalm, C. Huntingford, S. Sitch, A. Ahlström, A.Arneth, G. Camps-Valls, P. Ciais, P. Friedlingstein, F. Gans, K. Ichii, A. K. Jain, E. Kato, D. Papale, B. Poulter, B. Raduly, C. Rödenbeck, G. Tramontana, N. Viovy, Ying-Ping Wang, U. Weber, S. Zaehle and N. Zeng 2017 Compensatory water effects link yearly global land CO_2 sink changes to temperature. *Nature* 541 516-520.

Keenan, T. F., and A. D. Richardson 2015 The timing of autumn senescence is affected by the timing of spring phenology: implications for predictive models. *Glob. Change Biol* 21: 2634-2641.

Keenan, T. F., I. C. Prentice, J. G. Canadell, C. A Williams, H. Wang, M. Raupach and G. J. Collatz 2016 Recent pause in the growth rate of atmospheric CO_2 due to enhanced terrestrial carbon uptake. *Nat. Commun* 7 13428.

Keith W. Oleson, D. M. Lawrence, Gordon B. Bonan, M G. Flanner , E Kluzek , J. Peter , S. Levis , S. C. Swenson , E. Thornton , J. Feddema , C. L. Heald , J F. Lamarque , Guo-yue Niu , T. Qian , S. Running , K. Sakaguchi , L. Yang , X. Zeng , X. Zeng and M. Decker 2003 Technical Description of version 4.5 of the Community Land Model (CLM). NCAR Technical Note NCAR/TN-503+ STR, Boulder, Colorado.

Keeling, C. D., J. F. S. Chin, and T. P. Whorf. 1996 Increased activity of northern vegetation inferred from atmospheric CO_2 measurement. *Nature* 382 146-149.

Koven, C. D., B. Ringeval and P. Friedlingstein, 2011 Permafrost carbon-climate feedbacks accelerate global warming. *Proc. Nat Acad. Sci. USA* 108 14769-14774.

Krinner, G., N. Viovy, N. de Noblet-Ducoudré, 2005 A dynamic global vegetation model for studies of the coupled atmosphere-biosphere system. *Global. Biogeocheml. Cy* 19 1-33.

Liu, Q., Y. H. Fu, Z. Zhu, Y. Liu, Z. Liu, M. Huang, I. A. Janssens, and S. Piao. 2016. Delayed autumn phenology in the Northern Hemisphere is related to change in both climate and spring phenology. *Glob. Change Biol* 22 3702-3711.

Matthews, H. D., A. J. Weaver, K. J. Meissner, N. P. Gillett and M. Eby 2004 Natural and anthropogenic climate change: incorporating historical land cover change, vegetation dynamics and the global carbon cycle. *Clim Dynam* 22 461-479.

Masane K A and Tans PP 1955, Extension and Integration of atmospheric carbon of atmospheric carbon dioxide data into a globally consistent measurement record. *J Geophys Res- Atmos* 100 11593-11610.

McGuire, A. D., C. Koven, David M. Lawrence, J. S. Clein, J.Y. Xia, C. Beer, E. Burke, G. Chen, X. Chen, C. Delire, E. Jafarov, A. H. MacDougall, S. Marchenko, D. Nicolsky, S.S. Peng, A. Rinke, K. Saito, W. Zhang, R. Alkama, T. J. Bohn, P. Ciais, B. Decharme, A. Ekici, I. Gouttevin, T, Hajima, D. J. Hayes, D. Ji, G. Krinner, D. P. Lettenmaier, Y. Q. Luo, P. A.

Miller, John C. Moore, V. Romanovsky, C. Schädel, K. Schaefer, E A.G. Schuur, B Smith, T. Sueyoshi and Q. Zhuang 2016 Variability in the sensitivity among model simulations of permafrost and carbon dynamics in the permafrost region between 1960 and 2009. *Global. Biogeocheml. Cy* 30 1015-1037.

Montañez, I. P., J. C. McElwain, C. J. Poulsen, J. D. White, W. A. DiMichele, J. P. Wilson, G. Griggs and M. T. Hren 2016 Climate, pCO_2 and terrestrial carbon cycle linkages during late Palaeozoic glacial–interglacial cycles. *Nat. Geosci* 9 824-828.

Myneni, R. B, C. D. Keeling, C. J. Tucker, G. Asrar and R. R. Nemani 1997 Increased plant growth in the northern high latitudes from 1981 to 1991. *Nature* 386 698-702.

Peng, S., S. Piao, P. Ciais, R. B. Myneni, A. Chen, Frédéric Chevallier, A. J. Dolman, I. A. Janssens, J. Peñuelas, G. Zhang, S. Vicca, S. Wan, S. Wang and H Zeng 2013 Asymmetric effects of daytime and night-time warming on Northern Hemisphere vegetation. *Nature* 501 88-92.

Peng, S., F. Chevallier, P. Peylin, P. Cadule, S. Sitch, S. Piao, A. Ahlström, C. Huntingford, P. Levy, X. Li, Y. Liu, M. Lomas, B. Poulter, N. Viovy, T. Wang, X. Wang, S. Zaehle, N. Zeng, F. Zhao and H. Zhao 2015 Benchmarking the seasonal cycle of CO_2 fluxes simulated by terrestrial ecosystem models. *Global Biogeochem. Cycles* 29 46–64.

Peng, S., P. Ciais, G. Krinner, T. Wang, I. Gouttevin, A.D Mcguire, D. Lawrence, Burke, X. Chen, B. Decharme, C. Koven, A Macdougall, A. Rinke, K. Saito, W. Zhang, R. Alkama, T.J Bohn, C. Delire, T Hajima, D. Ji, D. P. Lettenmaier, P.A Miller, J.C. Moore, B. Smith and T Sueyoshi 2016 Simulated high-latitude soil thermal dynamics during the past 4 decades. *The Cryosphere* 10 179-192.

Peter, M. C 2001 Description of the TRIFFID dynamic global vegetation model. Hadley Centre technical note. 24 1-16.

Piao, S., J. Fang, L. Zhou, P. Ciais, and B. Zhu 2006 Variations in satellite-derived phenology in China's temperate vegetation. *Glob. Change. Biol* 12 672-685.

549 Piao, S., P. Ciais, P. Friedlingstein, P Peylin, M. Reichstein, S. Luyssaert, H. Margolis, J. Fang,
550 A. Barr, A. Chen, A. Grelle, David Y. Hollinger, T. Laurila, A. Lindroth, Andrew D.
551 Richardson and T. Vesala 2008 Net carbon dioxide losses of northern ecosystems in
552 response to autumn warming. *Nature* 451 49-52.

553 Piao, S., M. Cui, A. Chen, X.Wang, P. Ciais, J.Liu and Y. Tang 2011 Altitude and temperature
554 dependence of change in the spring vegetation green-up date from 1982 to 2006 in the
555 Qinghai-Xizang Plateau. *Agr. Forest. Meteorol* 151 1599-1608.

556 Piao, S., H. Nan, C. Huntingford, P. Ciais, P. Friedlingstein, S. Sitch, S. Peng, A. Ahlström, J.
557 G. Canadell, N. Cong, S. Levis, P. E. Levy, L. Liu, M. R. Lomas, J. Mao, R. B. Myneni, P.
558 Peylin, B. Poulter, X. Shi, G. Yin, N. Viovy, T. Wang, X. Wang, S. Zaehle, N. Zeng, Z.
559 Zeng and A. Chen 2014 Evidence for a weakening relationship between interannual
560 temperature variability and northern vegetation activity. *Nat. commun* 5 5018.

561 Piao, S., Z. Liu, Y. Wang, Y. Wang, P. Ciais, Y. Yao, S. Peng, F. Chevallier, P. Friedlingstein, I.
562 A. Janssens, J. Peñuelas, S. Sitch and T. Wang 2017a On the causes of trends in the seasonal
563 amplitude of atmospheric CO_2. *Glob. Change Biol* 00 1-9.

564 Piao, S., Z. Liu, T. Wang, S.Peng, P. Ciais, M. Huang, A. Ahlstrom, J. F. Burkhart, Frédéric
565 Chevallier, I. A. Janssens, Su-Jong Jeong, X. Lin, J. Mao, J. Miller, A. Mohammat, R. B.
566 Myneni, J. Peñuelas, X. Shi, A.Stohl, Y. Yao, Z. Zhu and P. P. Tans 2017b Weakening
567 temperature control on the interannual variations of spring carbon uptake across northern
568 lands. *Nature Clim. Change* 7 359-363.

569 Pinzon, J.E., and Tucker, C. J 2014 A Non-Stationary 1981-2012 AVHRR NDVI3g Time Series.
570 *Remote Sensing* 6 6929-6960.

571 Poulter, B., D. Frank, P. Ciais, R. B. Myneni, N. Andela, J. Bi, G. Broquet, J. G. Canadell, F.
572 Chevallier, Yi Y. Liu, Steven W. Running, S. Sitch and Guido R. vander Werf 2014
573 Contribution of semi-arid ecosystems to interannual variability of the global carbon cycle.
574 *Nature* 509 600-603.

575 Randerson, J. T., M. V. Thompson, T. J. Conway, I. Y. Fung, and C. B. Field. 1997 The

contribution of terrestrial sources and sinks to trends in the seasonal cycle of atmospheric carbon dioxide. *Global. Biogeocheml. Cy* 11 535-560.

Rawlins, M. A., A. D. McGuire, John S. Kimball, P. Dass, D. Lawrence, E. Burke, X. Chen, C. Delire, C. Koven, A. MacDougall, S. Peng, A. Rinke, K. Saito, W. Zhang, R. Alkama, Theodore J. Bohn, P. Ciais, B. Decharme, I. Gouttevin, T. Hajima, D. Ji, G. Krinner, Dennis P. Lettenmaier, P. MillerFollow, J. C. Moore, B. Smith and T. Sueyoshi 2015 Assessment of model estimates of land-atmosphere CO_2 exchange across Northern Eurasia. *Biogeosciences* 12 4385-4405.

Richardson, A. D., T. A. Black, P. Ciais, N. Delbart, M. A. Friedl, N. Gobron, D. Y. Hollinger, W. L. Kutsch, B. Longdoz, and S. Luyssaert 2010 Influence of spring and autumn phenological transitions on forest ecosystem productivity. *Philos TR SOC B* 365 3227-3246.

Richardson. A. D., R. S. Anderson, M. A. Arain, A. G. Barr, G. Bohrer, G. Chen, J. M. Chen, P. Ciais, K. J. Davis, A. R. Desai, M.C. Dietze, D. Dragoni, S. R. Garrity, C. M. Gough, R. Grant, David Y. Hollinger, H. A. Margolis, H. McCaughey, M. Migliavacca, R. K. Monson, J. W. Munger, B. Poulter, B. M. Raczka, D. M. Ricciuto, A, K. Sahoo, K. Schaefer, H. Tian, R. Vargas, H. Verbeeck, J. Xiao and Y. Xue 2012 Terrestrial biosphere models need better representation of vegetation phenology: results from the North American Carbon Program Site Synthesis. *Glob. Change Biol* 18 566-584.

Richardson. A. D., K Hufkens, T Milliman, D. M. Aubrecht, M. Chen, J. M. Gray, M. R. Johnston, T. F. Keenan, S. T. Klosterman, M. Kosmala, E. K. Melaas, M. A. Friedl and S. Frolking 2018 Tracking vegetation phenology across diverse North American biomes using PhenoCam imagery *Scientific data* 5 180028.

Rutishauser, T., J. Luterbacher, F. Jeanneret, C. Pfister and H. Wanner 2007 A phenology-based reconstruction of interannual changes in past spring seasons. *J. Geophys Res: Biogeo* 112 (G4).

Schleip, C., T. Rutishauser, J. Luterbacher and A. Menzel 2008 Time series modeling and central European temperature impact assessment of phenological records over the last 250

years. *J. Geophys Res: Biogeo* 113 (G4).

Schneising, O., M. Reuter, M. Buchwitz, J. Heymann, H. Bovensmann, and J. P. Burrows 2014 Terrestrial carbon sink observed from space: variation of growth rates and seasonal cycle amplitudes in response to interannual surface temperature variability. *Atmos Chem Phys* 14 133-141.

Sheffield, J., G. Goteti, and E. F. Wood 2006 Development of a 50-year high-resolution global dataset of meteorological forcings for land surface modeling. *J. Climate* 19 3088-3111.

Tanja, S., F. Berninger, T. Vesala, T. Markkanen, P. Hari, A. Mäkelä, H. Ilvesniemi, H. Hänninen, E. Nikinmaa, T. Huttula, T. Laurila, M. Aurela, A. Grelle, A. Lindroth, A. Arneth, O. Shibistova and J. Lloyd 2003 Air temperature triggers the recovery of evergreen boreal forest photosynthesis in spring. *Glob. Change Biol* 9 1410-1426.

Tjiputra, J.F, C. Roelandt, M. Bentsen, D. M. Lawrence, T. Lorentzen, J. Schwinger, Ø. Seland and C. Heinze 2013 Evaluation of the carbon cycle components in the Norwegian Earth System Model (NorESM). *Geosci. Model Dev* 6 301–325.

Thoning K. W., P. P. Tans and W. D. Komhyr 1989 Atmospheric carbon dioxide at Mauna Loa Observatory: 2. Analysis of the NOAA GMCC data, 1974–1985. *J. Geophys. Res.* 94 8549–8565.

Thoning, K. W., D. R. Kitzis, and A. Crotwell 2015 National Oceanic and Atmospheric Administration (NOAA), Earth System Research Laboratory (ESRL). *Global Monitoring Division (GMD): Boulder*, Colorado, USA. Version 2015-12.

Tucker, C. J 1979 Red and photographic infrared linear combinations for monitoring vegetation. *Remote Sens Environ* 8 127-150.

Tucker, C. J, J, J. E. Pinzon, M. E. Brown, D. A. Slayback, E. W. Pak, R. Mahoney, E. F. Vermote and Nazmi El Saleous 2005 An extended AVHRR 8-km NDVI dataset compatible with MODIS and SPOT vegetation NDVI data. *Int J. Remote Sens* 26 4485-4498.

Vesala, T., S. Launiainen, P. Kolari, J. Pumpanen, S. Sevanto, P. Hari, E. Nikinmaa, P. Kaski,

H. Mannila, E. Ukkonen, S. L. Piao and P. Ciais 2010 Autumn temperature and carbon balance of a boreal Scots pine forest in Southern Finland. *Biogeosciences* 7 163-176.

Vitassea, Y., C. Signarbieux, and Y H. Fu 2018 Global warming leads to more uniform spring phenology across elevations. *Proc. Natl Acad. Sci. USA* 115 1004-1008.

Wang, H., J.Dai, , Rutishauser, T., Gonsamo, A., Wu, C., and Ge, Q 2018 Trends and variability in temperature sensitivity of lilac flowering phenology. *J Geophys Res-Biogeo*. 123.

Wang, J., J. Dong, J. Liu, M. Huang, G. Li, S. W. Running, W. K. Smith, W. Harris, N. Saigusa, H. Kondo, Y. Liu, T. Hirano and X. Xiao 2014 Comparison of gross primary productivity derived from GIMMS NDVI3g, GIMMS, and MODIS in Southeast Asia. *Remote Sensing* 6 2108-2133.

Wang, X., S. Piao, X. Xu, P. Ciais, N. MacBean, R. B. Myneni and L. Li 2015 Has the advancing onset of spring vegetation green-up slowed down or changed abruptly over the last three decades? *Global Ecol. Biogeogr* 24 621-631.

Wenzel, S., P. M. Cox, V. Eyring, and P. Friedlingstein 2016 Projected land photosynthesis constrained by changes in the seasonal cycle of atmospheric CO_2. *Nature* 538 499-501.

Xia, J., J. Chen, S. Piao, P. Ciais, Y.Q.Luo and S. Wan 2014 Terrestrial carbon cycle affected by non-uniform climate warming. *Nat Geosci* 7 173.

Xia, J., A. D. McGuire, D.Lawrence, E. Burke, G.S. Chen, X. D. Chen, C. Delire, C. Koven, A. MacDougall, S.S. Peng, A. Rinke, K. Saito, W. X. Zhang, R. Alkama, Theodore J. Bohn, P. Ciais, B. Decharme, I. Gouttevin, T. Hajima, D. J. Hayes, K. Huang, D. Ji, G. Krinner, D. P. Lettenmaier, P. A. Miller, John C. Moore, Benjamin Smith, T. Sueyoshi, Z. Shi, L. Yan, J Liang, L. Jiang, Q. Zhang and Y. Luo 2017 Terrestrial ecosystem model performance in simulating productivity and its vulnerability to climate change in the northern permafrost region. *J Geophys Res-Biogeo*, 122 430-446.

Xu, L., R. B. Myneni, F. S. Chapin III, T. V. Callaghan, J. E. Pinzon, C. J. Tucker, Z. Zhu, J. Bi, P. Ciais, H. Tømmervik, E. S. Euskirchen, B. C. Forbes, S. L. Piao, B. T. Anderson, S. Ganguly, R. R. Nemani, S. J. Goetz, P. S. A. Beck, A. G. Bunn, C. Cao and J. C. Stroeve

2013 Temperature and vegetation seasonality diminishment over northern lands. *Nat Clim Change* 1758-678X.

Yuan, W., S. Piao, D. Qin, W. Dong, J. Xia, H., Lin and M. Chen. 2018 Influence of vegetation growth on the enhanced seasonality of atmospheric CO_2. *Global Biogeochemical Cycles* 32 32–41.

Yu, H., E. Luedeling, and J. Xu. 2010 Winter and spring warming result in delayed spring phenology on the Tibetan Plateau. *Proc. Natl Acad. Sci. USA* 107 22151-22156.

Zeng, N., F. Zhao, G. J. Collatz, E. Kalnay, R. J. Salawitch, T. O. West and L. Guanter 2014 Agricultural green revolution as a driver of increasing atmospheric CO_2 seasonal amplitude. *Nature* 515 394-397.

Zhang, G., Y. Zhang, J. Dong, and X. Xiao 2013 Green-up dates in the Tibetan Plateau have continuously advanced from 1982 to 2011. *Proc. Natl Acad. Sci. USA* 110 4309-4314.

Zhou, L., C. J. Tucker, R. K. Kaufmann, D. Slayback, N. V. Shabanov, R. B. Myneni 2001 Variations in northern vegetation activity inferred from satellite data of vegetation index during 1981 to 1999. *J. Geophys Res: Atmosph* 106 20069-20083.

Figures

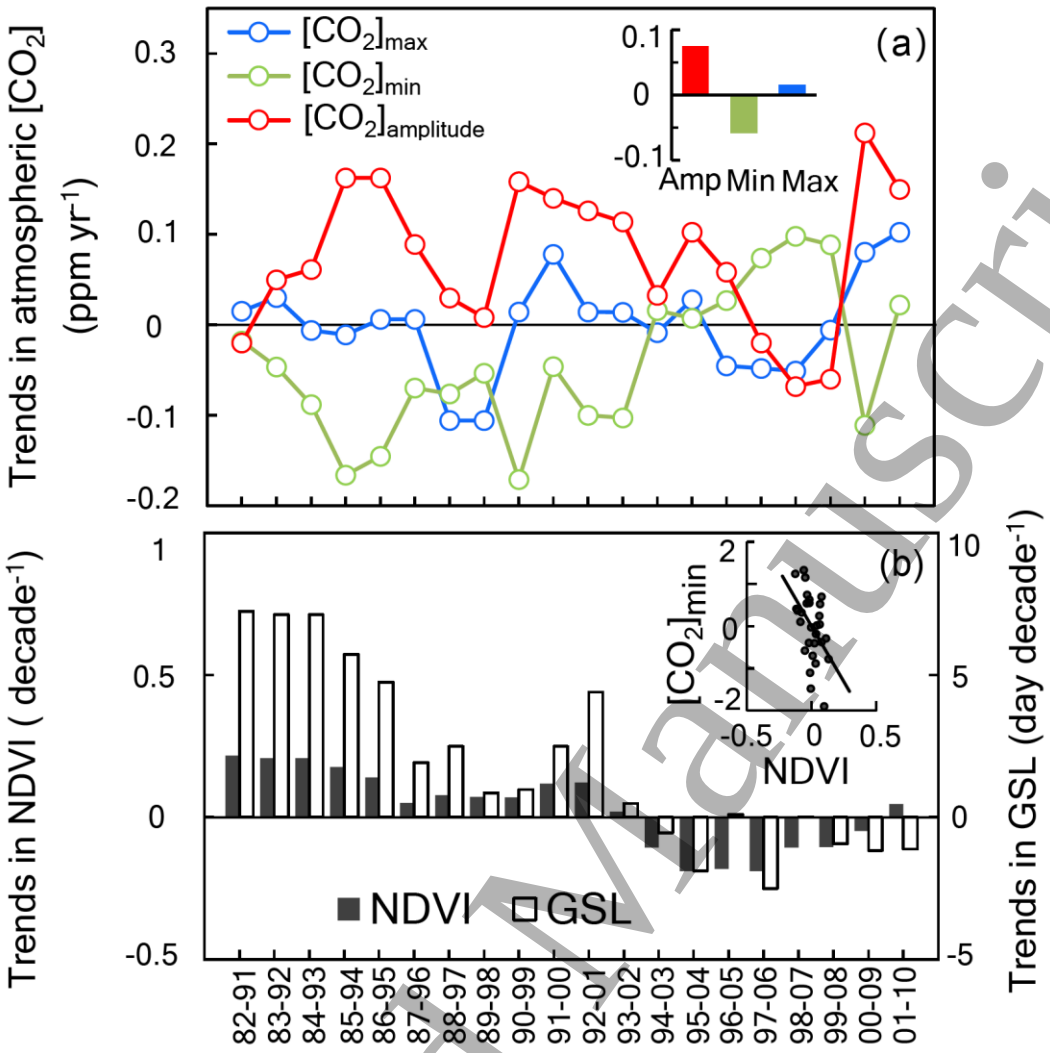

Figure 1. Changes in temporal trends of CO_2 amplitude and plant growth (NDVI). 10-year moving window from 1982 to 2010 show the changing trends of (**a**), the peak-to-trough amplitude ($[CO_2]_{amplitude}$) and yearly maximum CO_2 concentration ($[CO_2]_{max}$) as well as the minimum CO_2 concentration ($[CO_2]_{min}$) at Point Barrow (BRW); (**b**) NDVI and growing season length (GSL). The insert in panel A represents changing rates of the $[CO_2]_{amplitude}$, $[CO_2]_{max}$ and $[CO_2]_{min}$ during 1982-2010. The insert in panel (a) shows the long-term trends of $[CO_2]_{amplitude}$ (red column, 0.075 ppm yr^{-1}, P<0.01), $[CO_2]_{min}$ (green column, -0.058 ppm yr^{-1}, P<0.01) and $[CO_2]_{max}$ (blue column, 0.016 ppm yr^{-1}, P =0.17) across 1982 to 2010. The insert in panel (b) shows the correlation between the yearly anomalies of the $[CO_2]_{min}$ and NDVI during 1982-2010 (with r = -0.47, P <0.05).

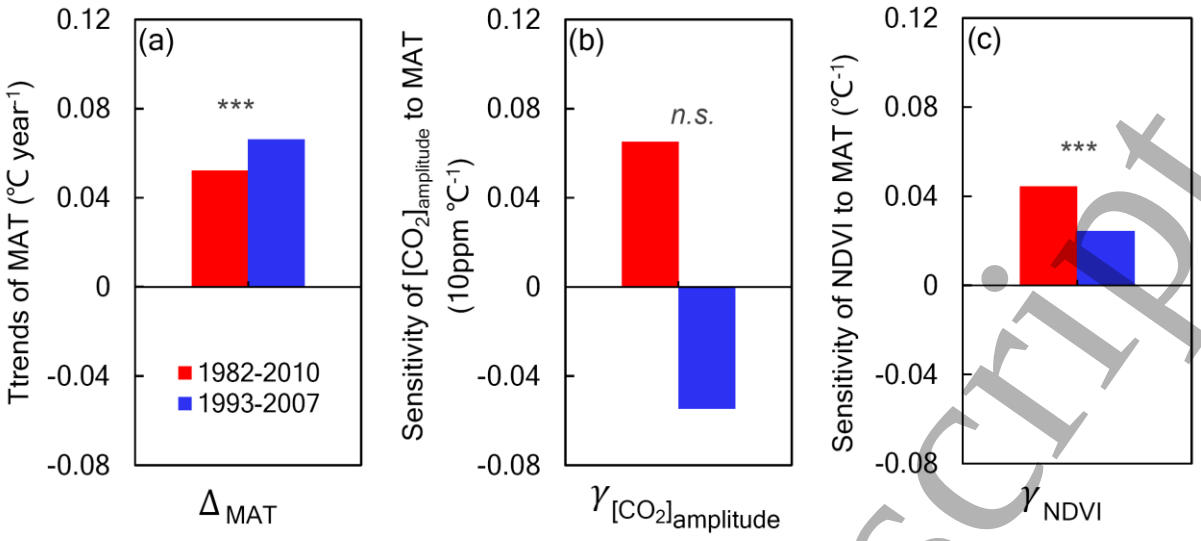

Figure 2. The changes of mean annual temperature (a. ΔMAT, °C year^{-1}) and the temperature sensitivities of atmospheric CO_2 seasonal amplitude (b. $\gamma_{[CO_2]amplitude}$, 10ppm °C^{-1}) and of the NDVI (c. γ_{NDVI}, °C^{-1}) during 1982-2010 and 1993-2007. ***Significant difference at P <0.01, and *n.s.* represents no significance.

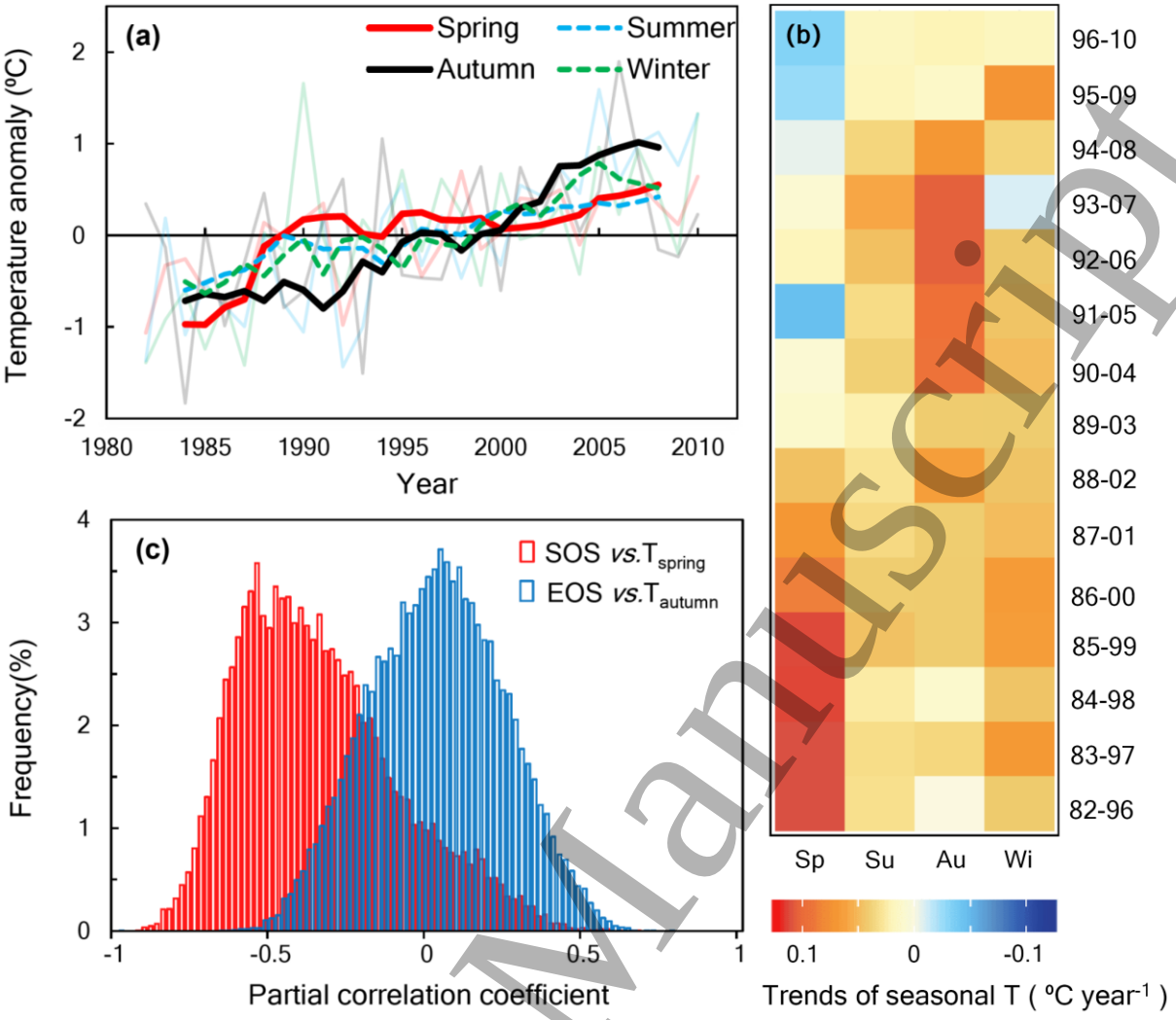

Figure 3. Temporal variations of seasonal temperature over northern lands (>50°N). (**a**) The year-to-year anomalies were shown by the transparent lines and their 5-year running means were displayed by the solid (spring and autumn) and dashed lines (summer and winter). (**b**)15-year moving windows from 1982 to 2010 show the trends of seasonal temperature changes. (**c**) Frequency histograms of the sensitivity (i.e., the partial correlation coefficient) of SOS to spring temperature change (SOS vs. T_{spring}) and EOS to autumn temperature change (EOS vs. T_{autumn}) from 1982 to 2010. Note that the negative values of the *X*-axis represent the advanced SOS or EOS with temperature increase.

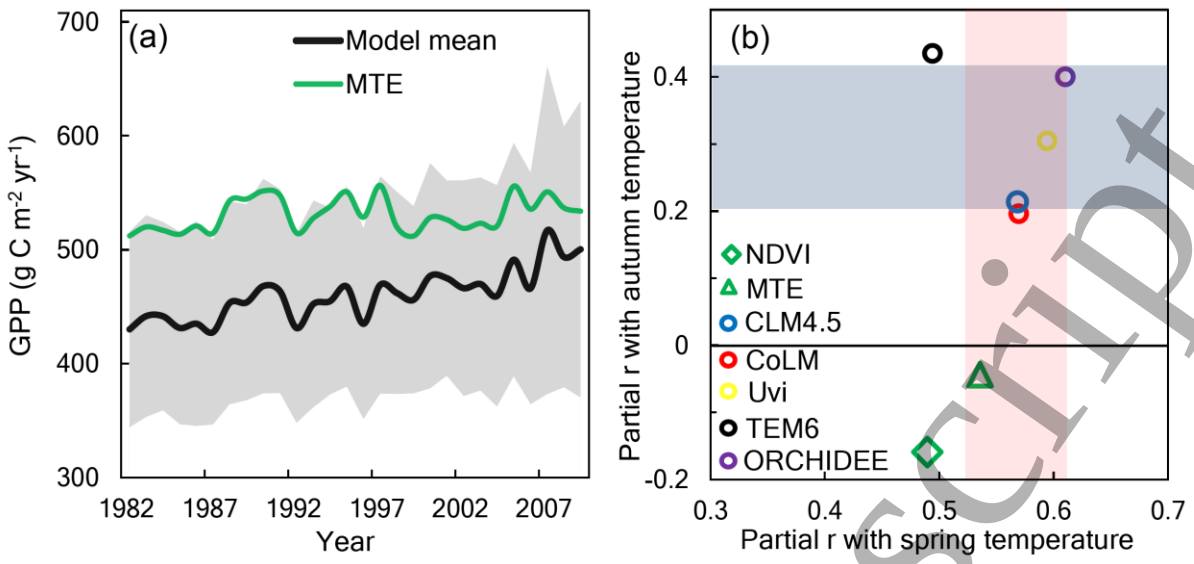

Figure 4. Temporal variations of GPP and its dependence on spring and autumn temperature. (**a**) Temporal changes of annual total GPP over northern lands (>50ºN) from a flux-based dataset (i.e., MTE) and five terrestrial biosphere models (See Methods). The green line show the annual MTE GPP. The black line represents the model averages and the grey area is the standard deviation among models. (**b**) Mean partial correlation coefficient (partial *r*) of NDVI and GPP to spring temperature and autumn temperature changes. The shaded areas represent the standard deviations of the partial *r* among models. Note that only the grid cells with significant partial correlation (P <0.05) were included in this analysis.